Neutron-diffraction study of the magnetic ordering in the insulating regime of the perovskites RNiO$_3$ (R = Pr and Nd)

J. L. García-Muñoz

Institut Laue-Langevin, Boîte Postale 156, 38042 Grenoble Cedex 9, France
and Instituto de Ciencia de Materiales de Barcelona (CSIC), 08193 Bellaterra, Spain

J. Rodríguez-Carvajal

Laboratoire Léon Brillouin, Commissariat à l'Energie Atomique et Centre National de la Recherche Scientifique,
Centre d'Etudes de Saclay, 91191 Gif-sur-Yvette Cedex, France
and Institut Laue-Langevin, Boîte Postale 156, 38042 Grenoble Cedex 9, France

P. Lacorre*

IBM Research Division, Almaden Research Center, 650 Harry Road, San José, California 95120-6099
(Received 8 November 1993)

Neutron-diffraction experiments and polarization analysis techniques reveal that the metal-insulator transition in the orthorhombic perovskites PrNiO$_3$ and NdNiO$_3$ is accompanied by a sudden three-dimensional magnetic ordering of the Ni sites ($\mu_{Ni} \approx 0.9\mu_B$). The electronic localization is followed by a magnetic ground state consisting of an unusual antiferromagnetic structure, with $\mathbf{k} = (\frac{1}{2}, 0, \frac{1}{2})$ relative to the orthorhombic crystal cell. This propagation vector implies the symmetrical coexistence of ferro- and antiferromagnetic couplings along the three pseudocubic axes. This suggests the existence of a nonuniform orbital distribution of the single e_g electron. The orbital superlattice may result from the breakdown of the degeneracy of the Ni^{III}($t_{2g}^6 e_g^1$) state due to electronic correlation. This type of spin arrangement has not been observed in other perovskite oxides. These findings are confirmed by the magnetic behavior of the single crystallographic Nd site: half of these ions become ordered and the other half remain disordered as in a simple paramagnet. This can be explained by the combination of polarization effects due to the exchange field from nickel moments and the breaking down of point symmetry at Ni site.

I. INTRODUCTION

In a previous paper dealing with the structure aspects of the nickel perovskites RNiO$_3$ (R =La, Pr, Nd, and Sm), we reported[1] the existence of electronically induced structural changes associated with the metal-insulator (M-I) transition recently discovered in these oxides.[2] In Ref. 1, we gave evidence for a very subtle increase of the Ni-O bondlength ($\Delta d_{Ni-O} \approx +0.004$ Å) going through the transition which accounts for the change in the unit-cell volume ($\Delta V / V_{metal} \approx 0.25\%$) and the changes of the bent Ni-O-Ni angle. Such a subtle variation of the orthorhombic distortion at the transition takes place apparently without any change in the crystallographic *Pbnm* symmetry (within the resolution of our neutron-diffraction data). In Ref. 1, we concentrated on the analysis of the structural anomalies at the electronic transition without considering the magnetic behavior. The high-resolution neutron-diffraction studies have been completed with polarized neutron experiments. The goal of these measurements is to bring out information on the magnetic behavior of these compounds in order to approach the nature of the first-order breakdown of the metallic regime. Here, we report the detailed results on the magnetic properties of PrNiO$_3$ and NdNiO$_3$ below the electronic transition. The unexpected findings are valuable information in any attempt to explain the nature of the band gap, and to build up the electronic ground state in these oxides.

The fundamental electronic energies determining the conductivity and band gaps of 3d transition-metal (TM) compounds have been a controversial topic since 1973 when Boer and Verwey[3] pointed out that standard one-electron band theory breaks down in predicting the insulating state of many of these compounds. The discovery of superconductivity in copper oxides has stimulated a very intense effort in order to get an overall understanding of their basic electronic processes. Actually, both Coulomb correlations within the TM 3d bands (Mott-Hubbard gap), and screening effects by charge transfer from the anion p bands (charge-transfer gap) in oxides, halides, and sulfides are included in the framework developed by Zaanen, Sawtzky, and Allen.[4] According to this emerging picture, Torrance et al.,[5] studied a large number of TM oxides by using a simple ionic model in order to estimate the differences between the two relevant energies (Δ, the charge-transfer energy, and U, the correlation energy). The estimations for classical examples of proposed Mott-Hubbard compounds as V$_2$O$_3$, Ti$_2$O$_3$ Ti$_2$O$_3$ or RTiO$_3$ (R, rare earth), appear well located near the boundary which separates small-U insulators and metals. However, for the RNiO$_3$ compounds, the differences between Δ and U values locate them very close to the boundary separating "low-Δ metals"

($\Delta < W$=dispersional bandwidth) from "charge-transfer insulators" ($W < \Delta < U$). Such estimations are found to be consistent with the discovery of a first-order metal-insulator transition in nickel perovskites with $R = $Pr, Nd, Sm, and Eu, in which the transition temperatures strongly decreases as the size of the rare-earth cation increases. According to Refs. 1, 6, and 7 the transition could be related to the opening of a $d^7\underline{L}$-d^8 charge-transfer gap by virtue of important covalent transfer between metal $3d$ and anion p states. As pointed out in Refs. 1 and 7, the thermally driven straightening out of the Ni-O-Ni angle in RNiO$_3$ should lead to the overlap of the upper and lower subbands around E_F and the gap closing above T_{MI} (the metal-insulator transition temperature).

A mechanism, the "negative charge-transfer gap," has been proposed recently in connection with the photoemission spectra of NaCuO$_2$.[8] Calculations by Mizokawa et al. are consistent with a negative $d^n \rightarrow d^{n+1}\underline{L}$ charge-transfer energy for some formally trivalent oxides, which results in a ground state dominated by a $d^{n+1}\underline{L}$ configuration. Thus, a $d^8\underline{L}$ configuration (instead of $d^7[\text{Ni}^{3+}]$) has been invoked also in relation to some nickelates such as LiNiO$_2$ or RNiO$_3$ (see for instance Refs. 8 and 9). As hinted by the analysis of photoemission spectra of Li-doped NiO,[10] the possibility of a $d^8\underline{L}$ configuration requires further investigation.

Concerning the magnetic behavior of RNiO$_3$, little is known. Demazeau et al.[11] reported a maximum in the susceptibility of the insulators YNiO$_3$ ($T_N = 145$ K) and LuNiO$_3$ ($T_N = 130$ K). In Ref. 7, μ^+ spin rotation was used to determine the evolution of the magnetic ordering temperature with the rare-earth size, showing that the magnetic transition is driven by the M-I transition for Pr and Nd rare earths, but is independent of it for Sm and smaller rare earths. This paper gives a complete description of the magnetic structures and magnetic behavior of PrNiO$_3$ and NdNiO$_3$ as revealed by neutron-diffraction experiments. A short first account of the magnetic behavior of the nickel sublattice was given in Ref. 12. All the points concerned with the crystal structure have been thoroughly discussed in Ref. 1 and will not be repeated here. In the present article we give a more detailed analysis of the unexpected magnetic ordering of Ni ions, which has been confirmed by the study of the magnetic behavior of the rare-earth sublattices.

The paper is organized as follows: Sec. II is devoted to experimental details about neutron experiments. The magnetic nature of the extra weak diffraction peaks appearing below the metal-insulator transition is shown in Sec. III, and interpreted in terms of an unusual magnetic ordering of Ni moments in Secs. IV and V. The details of the magnetic structure determination are presented in the Appendix. Finally, in Secs. VI and VII, we discuss the implications of the magnetic structure on the electronic structure of Ni ions.

II. EXPERIMENT

PrNiO$_3$ and NdNiO$_3$ powder samples were the same as those in Ref. 1. The results reported in this paper come from two types of experiments at the Institut Laue-Langevin in Grenoble (France): (i) neutron-diffraction measurements on the high-flux powder diffractometer D1B ($\lambda = 2.52$ Å) from 1.5 K to room temperature and (ii) polarized neutron diffraction in the triple-axis spectrometer IN20 ($\lambda = 2.34$ Å). D1B was used to follow the thermal evolution of the main magnetic reflections because of its resolution at low scattering angles and the fixed position of its position sensitive detector. The details about D1B experiments have been already described in Ref. 2.

IN20 is equipped for polarization analysis, allowing the separation of magnetic scattering. A Heusler polarizer monochromator providing an incident energy of 14.9 meV ($\lambda = 2.34$ Å) was used. A pyrolytic graphite filter removes high-order ($\lambda/2$) contamination. Variable curvature horizontally magnetized Heusler [111] crystals were used either as monochromator polarizer and analyzer. A small magnetic field (~ 15 Oe) was imposed at the sample position, and its direction fixed to be always parallel to the momentum transfer (P$\|$Q). With this geometry, magnetic scattering produces the spin inversion of the polarized incoming neutrons, contributing to the spin-flip (SF) channel.

The data from D1B measurements were analyzed following the Rietveld method by using the STRAP package programs.[13] In particular we used the program FULLPROF[14] for both single and sequential refinements. The evolution of the magnetic parameters was obtained from sequential refinements where the nuclear structure variation was also included.

III. MAGNETIC ORIGIN OF THE SMALL DIFFRACTION PEAKS IN THE INSULATING REGIME

Diffraction patterns revealed the presence of very weak reflections below T_{MI} in PrNiO$_3$ and NdNiO$_3$ (see also Refs. 1 and 2). They completely vanish at T_{MI} and are no longer visible in the metallic regime. As shown in Figs. 1 (PrNiO)$_3$ and 2 (NdNiO$_3$), they can be indexed with integer indices in a lattice with doubled a and c axes relative to the orthorhombic crystal cell ($a = 5.389$ [5.419], $b = 5.382$ [5.380], $c = 7.610$ [7.626] Å for PrNiO$_3$ [NdNiO$_3$]); these superlattice reflections are defined by the wave vector $\mathbf{k} = (\frac{1}{2}, 0, \frac{1}{2})$, belonging to the point T of the Brillouin zone (space group $Pbnm$). In order to investigate their nature, polarization analysis experiments were conducted as described above. Because of the P$\|$Q geometry used, any single magnetic scattering process is counted in the spin-flip (SF) channel. Measurements were performed around the most intense reflections [$(\frac{1}{2}, 0, \frac{1}{2})$, $(\frac{1}{2}, 1, \frac{1}{2})$, and the nuclear (1,1,0)] at 1.5 K and 100 K for NdNiO$_3$, and at 1.5 K for PrNiO$_3$. The results, after being corrected for the flipping ratio ($R_0 = 13$), are shown in Figs. 3 and 4. In these figures the $(\frac{1}{2}, \frac{1}{2}, \frac{1}{2})$ magnetic reflection from the small amount of NiO ($< 2\%$), included as an impurity phase in the refinements, is also present.

Two conclusions can be drawn from Figs. 3: First, they prove the magnetic origin of the superlattice $\mathbf{k} = (\frac{1}{2}, 0, \frac{1}{2})$ below T_{MI}; and, second, the flat non-spin-flip

signal (NSF) at the $(\frac{1}{2},0,\frac{1}{2})$ and $(\frac{1}{2},1,\frac{1}{2})$ positions confirms the absence of any significant nuclear-scattering contributing to them. Therefore, the only detected structural changes are those described in Ref. 1. Within this context, it is also interesting to note that the appearance of identical magnetic features just below T_{MI} (see Figs. 1 and 2) reveals the same magnetic ordering in both compounds.

Furthermore, there are changes in the diffraction intensities of the Nd compound below $T \sim 30$ K (Figs. 2 and 4). As previously proposed by Lacorre et al.,[2] they correspond to the magnetic ordering of the Nd sublattice and will be described later. We would first like to focus our attention on the problem of the magnetic order of the transition metal.

IV. MAGNETIC ORDER OF Ni MOMENTS

The arrangement of magnetic moments has been found with the help of group-theoretical calculations. In the Appendix the search for the possible magnetic structures in $PrNiO_3$ and $NdNiO_3$ is thoroughly detailed. The vector $\mathbf{k}$ lies on the surface of the first Brillouin zone and has the full symmetry of the space group $(G_{\mathbf{k}}=Pbnm)$. The

group of the propagation vector has only two irreducible bidimensional representations (see Table III) and the corresponding basis functions for the Ni sublattices can be written in terms of the magnetic modes given in Table IV.

In the case of $PrNiO_3$, several magnetic structures, obtained by linear combinations of the basis functions given in Table IV, fit the experimental diffraction pattern correctly. This is due to the weakness of the magnetic reflections as well as to some intrinsic degeneracy discussed in the Appendix. However, the consideration that the spin arrangement of Ni sublattices should be similar to that of $NdNiO_3$, where Nd ions order at low temperature, leads us to prefer a magnetic structure that is very close to $(F_x,0,0)$. That is the first partner of the basis function of the first representation with null magnetic components parallel to the y and z axes. Ni moments within the crystallographic unit cell are ferromagnetically aligned and parallel to x. The magnetic moments of the unit cell with origin at $\mathbf{R}$ are inverted according to the phase factor $\exp\{2\pi i\mathbf{k}\mathbf{R}\}$. The same alignment but with the spins pointing parallel to z (namely F_z) also fits correctly the data. However, the magnetic intensities of $NdNiO_3$, once Nd becomes ordered, can only be reproduced, with the Ni moments nearly aligned parallel to x, and therefore the F_z mode appears unlikely in $PrNiO_3$ and can be rejected. The fit to the experimental patterns

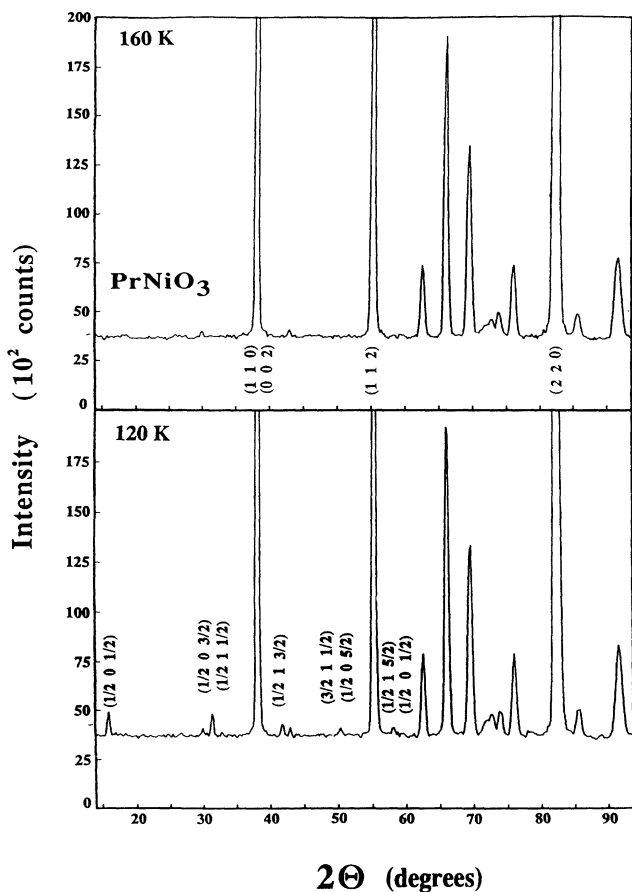FIG. 1. Portions of neutron-diffraction patterns of $PrNiO_3$, above (160 K) and below (120 K) the electronic transition temperature ($T_{\mathrm{MI}}=135$ K). The y-axis scale (intensity) has been expanded to show the weak reflections in the insulating regime.
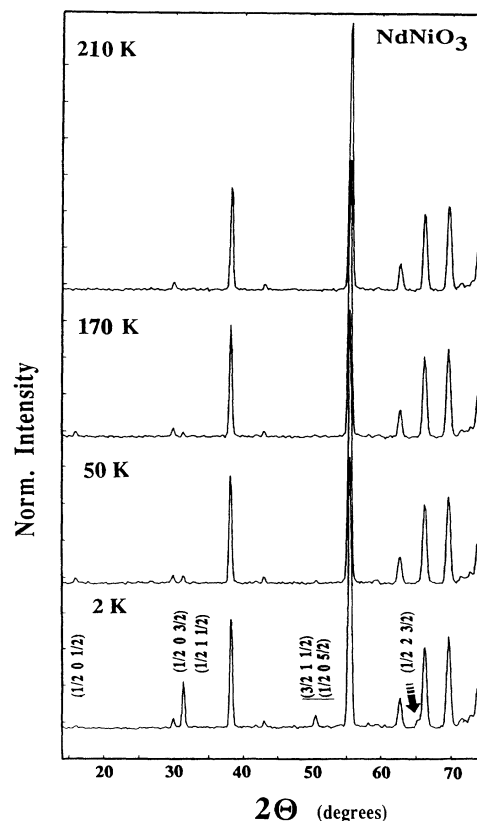
FIG. 2. Diffraction patterns of $NdNiO_3$ showing the appearance of the $\mathbf{k}=(\frac{1}{2},0,\frac{1}{2})$ weak reflections below $T_{\mathrm{MI}}=200$ K and their evolution at low temperatures (see explanation in the text).

by considering the F_x magnetic order are shown in Figs. 5(a) (PrNiO$_3$ at 1.5 K) and 5(b) (NdNiO$_3$ at 50 K). The saturated magnetic moments of Ni sites for PrNiO$_3$ and NdNiO$_3$ are, respectively, 0.93(1) and 0.92(5)μ_B/Ni ion. The usual nuclear and magnetic agreement factors are given in Table I.

An important result is the saturated ordered moment being very close to $1\mu_B$ per Ni ion in PrNiO$_3$ and NdNiO$_3$; that is, consistent with the low-spin Ni^{III} ($S=\frac{1}{2}$) state for nickel. The possibility of high-spin Ni^{2+} and holes at oxygens has also been examined. We have considered the alternative of magnetic holes "shared" by

all the oxygens in a wide $2p$ band. But such a situation would imply a magnetic form factor for anions ($\mu f = n_p \langle j_0 \rangle_{2p}$, where n_p is the effective number of unpaired electrons in $2p$ orbitals), falling down much more rapidly with scattering angle than that of Ni^{III} or Ni^{2+}. Therefore, magnetic moments at oxygen sites would contribute mainly to the first magnetic reflection ($\frac{1}{2},0,\frac{1}{2}$). As no significant deviation from the intensity calculated assuming the spherical form factor of Ni^{III} has been detected, there is no reason to suppose that the situation described above exists. However, we have also checked whether a "localized" magnetic moment on the oxygen
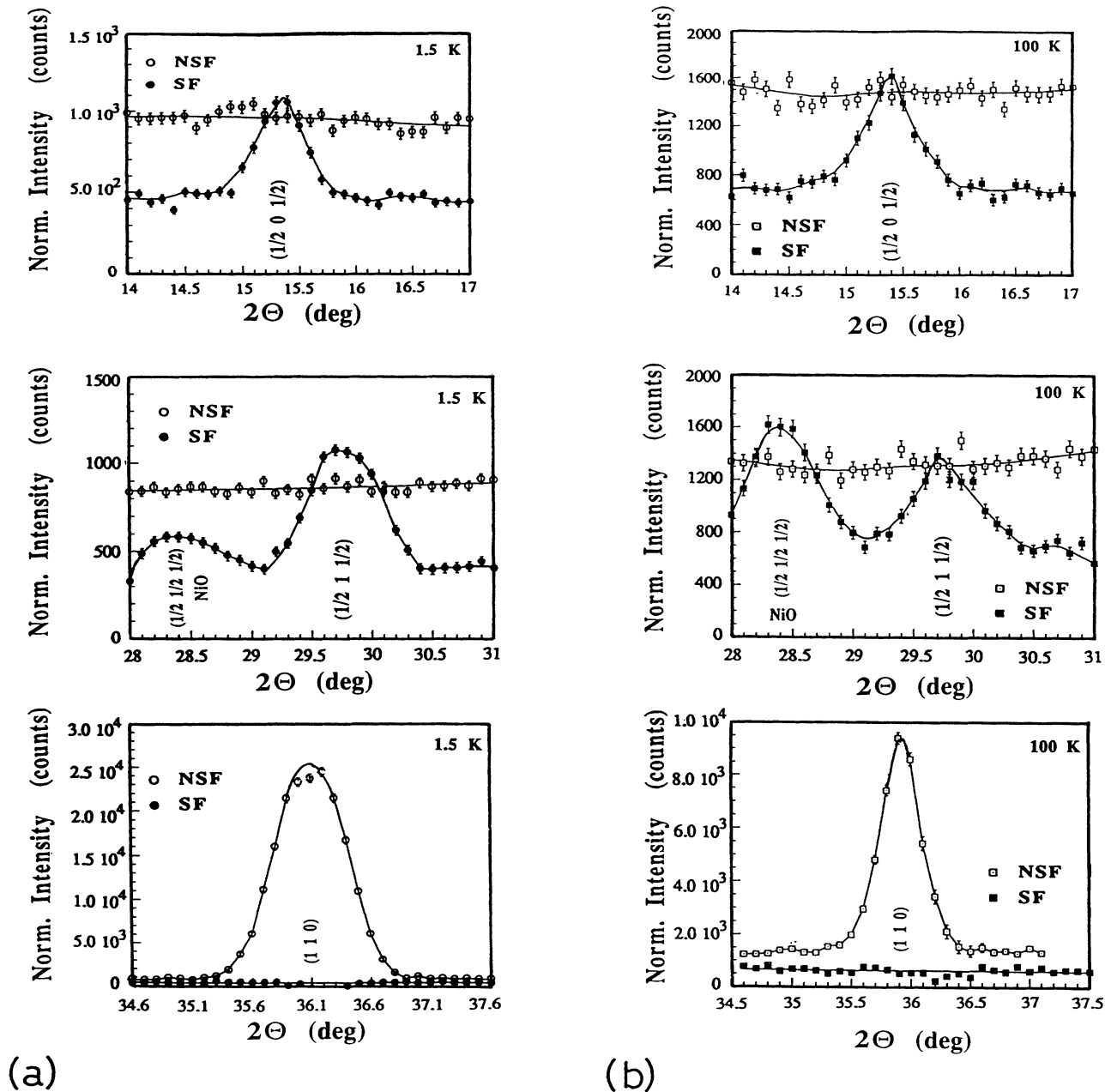

(a)   (b)

FIG. 3. Polarized beam diffraction patterns around ($\frac{1}{2},0,\frac{1}{2}$), ($\frac{1}{2},1,\frac{1}{2}$) and the nuclear (1,1,0) angular positions in (a) PrNiO$_3$ (1.5 K) and (b) NdNiO$_3$ (100 K). The difference between spin-flip (SF) and non-spin-flip (NSF) signals in the former probes their magnetic origin. Note the different scale for the strong nuclear reflection.

bridging a pair of ferromagnetically coupled "Ni^{2+}" could exist. The refinement converges to a negligible magnetic moment on the oxygen sites and the moment of Ni ions goes to $0.9\mu_B$. In addition, if the magnetic moment at Ni sites is fixed to $2\mu_B$, and only the oxygen moments are refined, a very poor reliability index ($R_{Mag} \approx 70\%$) is obtained.

Furthermore, the possibility of a non-equal-moment magnetic structure was also checked and a solution of this type was found in $PrNiO_3$. But, as extensively discussed in the Appendix, the consideration of the combined magnetic order of Nd and Ni in $NdNiO_3$ (see Table II and Appendix) leads us to prefer the Ni equal-moment structure as the actual physical solution in both compounds.

The magnetic structure (Fig. 6) can be described as alternating layers perpendicular to [001]: $A^+A^+A^-A^-A^+A^+A^-A^-A^+A^+ \cdots$, where the moments within one nickel A layer are perpendicular to

(a) 2Θ (deg)
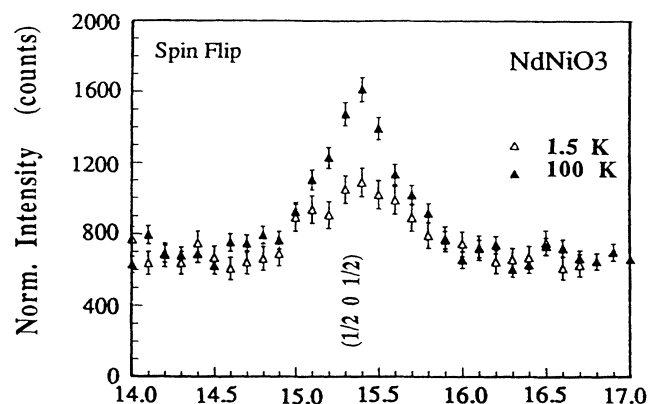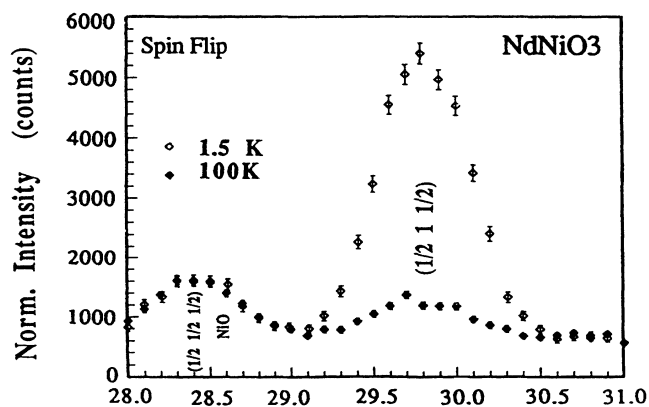
(b) 2Θ (deg)

FIG. 4. Comparison of the 1.5 and 100 K spin-flip signals in $NdNiO_3$ for (a) the $(\frac{1}{2},0,\frac{1}{2})$ and (b) $(\frac{1}{2},1,\frac{1}{2})$ magnetic reflections (see explanation in the text).

the bc plane and ordered as shown in Fig. 6. In Ni layers labeled "A^-" all the spins are inverted with respect to the "A^+" ones. Another way to visualize the magnetic structure is to consider it as a stacking $(++--++--)$ of "ferromagnetic planes" perpendicular to the pseudocubic direction $[111]_c$. The atomic Ni planes are parallel to the lattice planes $(101)_0$, i.e., perpendicular to the propagation vector. As far as we know, this magnetic ordering has not been observed before in an oxide with perovskite structure.

Figure 7 shows the thermal evolution of the magnetic moments in the Ni sublattice down to 1.5 K as obtained from sequential refinements. Since measurements were performed while continuously increasing temperature, the disappearance of magnetic order concomitant with the electronic delocalization is even sharper than that represented in this figure. Thus, what Fig. 7 represents is the first-order formation of localized moments at nickel sites when decreasing temperature. In $PrNiO_3$ and $NdNiO_3$ they order as soon as these compounds become insulators: in $PrNiO_3$ TM moments are completely saturated to $\sim 1\mu_B$ (Ni^{III} low spin) below T_{MI} ($T_{MI}=135$ K), whereas in $NdNiO_3$ ($T_{MI}=200$ K) they are fully saturated only below ~ 160 K, confirming that the virtual Néel temperature (T_N) is actually higher than T_{MI}. The thermal evolution close to the M-I transition in $NdNiO_3$ (Fig. 7) suggests a virtual Néel temperature located somewhere in the temperature range between 210 and 250 K.

V. MAGNETIC BEHAVIOR OF RARE-EARTH CATIONS

Figures 2 and 4 show significant variations in the intensity of $(\frac{1}{2},0,\frac{1}{2})$, $(\frac{1}{2},0,\frac{3}{2})$, $(\frac{1}{2},0,\frac{5}{2})$, and $(\frac{1}{2},2,\frac{3}{2})$ magnetic reflections in $NdNiO_3$, occurring below ~ 30 K. Obviously these changes arise from the ordering of Nd magnetic moments: such a phenomenon at such high temperatures has already been observed in Nd_2NiO_4 (Ref. 15) and is mainly due to the polarization of Nd^{3+} moments in the presence of the exchange field from nickel, rather than from the Nd-Nd interactions.

As the rare earth is located between two planes of Ni octahedra, there are eight nearest Ni neighbors around each Nd atom (four above and four below). By looking at Figs. 6 and 8, two different resultant exchange fields at the only crystallographic position occupied by neodymium can be distinguished: (i) for those Nd^{3+} ions in between A^+-A^+ or A^--A^- nickel layers, the net exchange field created by the nickel moments is non-null. We call those Nd layers B^+ and B^-, respectively (again, "$+$", "$-$" represent inverted moments). (ii) However, the situation is completely different for the remaining half of Nd ions, those Nd which occupy positions between A^+-A^- [or A^--A^+] magnetically ordered nickel layers. For them, the expected exchange field is close to zero or vanishingly small. We call these Nd layers B^0. Both, $B^\pm$ and B^0-type layers are displayed in Fig. 8.

In agreement with this analysis, the measurements reveal that only half of Nd moments are ordered: $\frac{1}{4}$ of the total correspond to Nd layers of type B^+ and the remaining $\frac{1}{4}$ to B^-. The other half of Nd^{3+} moments (at B^0-
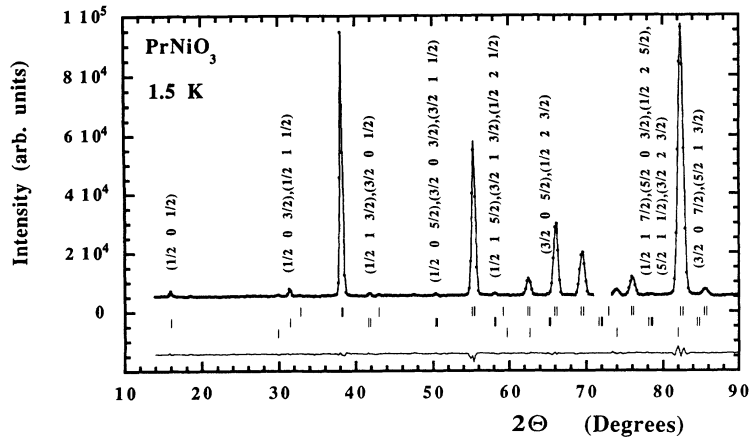
(a)
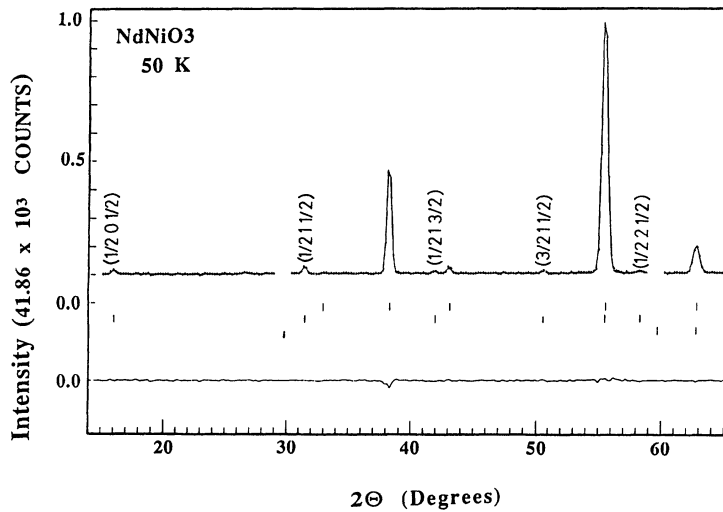
(b)

FIG. 5. Observed ($\bigcirc$) and calculated (———) neutron-diffraction patterns (a) $PrNiO_3$ at 1.5 K and (b) $NdNiO_3$ at 50 K. The main weak reflections developed across the M-I transition are labeled. The second row of reflections markers corresponds to the magnetic reflections of $RNiO_3$ and the third row to NiO.

type layers) remain disordered and behave as simple paramagnets.

This curious situation for a structure having only one Nd crystallographic site ($Pbnm$ space group) is the consequence of the breaking down of symmetry manifested by the particular magnetic order of Ni and is imposed by the propagation vector $\mathbf{k}=(\frac{1}{2},0,\frac{1}{2})$. Experimentally, $J_{\mathrm{Nd\text{-}Ni}}<0$ (antiferromagnetic coupling, see Fig. 8).

The magnetic structure of neodymium sublattices (Fig. 8) can be represented by the basis function $(V_x^-,0,V_z^-)$ (see the Appendix), from the first irreducible repre-

TABLE I. Magnetic structures of $PrNiO_3$ and $NdNiO_3$ and agreement factors.

Temperature	$NdNiO_3$ 50 K	$NdNiO_3$ 1.5 K	$PrNiO_3$ 1.5 K
Ni ions:			
(F_x,C_y,G_z):	[0.94(4),0,0]	[0.89(4),0,−0.14(6)]	[0.93(1),0,0]
m_T (Ni):	$0.94(4)\mu_B$	$0.92(5)\mu_B$	$0.93(1)\mu_B$
R ions:			
(V_x^-,V_y^+,V_z^-):		[2.05(8),0,−0.48(10)]	
$m_T(R_{1,4})(B^{\pm}$ layers)		$2.11(10)\mu_B$	
$m_T(R_{2,3})(B^0$ layers)		0	
R_N (%)	4.96	4.57	5.01
R_{MAG} (%)	8.4	9.6	8.5
χ^2	2.49	2.77	2.43

sentation $\Psi_1(T_1)$ of $G_{\mathbf{k}=(\frac{1}{2},0,\frac{1}{2})}$: being $\mathbf{V}^- = \mathbf{m}_1 - \mathbf{m}_4$, $m(\mathrm{Nd}_1) = m(\mathrm{Nd}_4)$, and $m(\mathrm{Nd}_2) = m(\mathrm{Nd}_3) = 0$.

Including this model in structure factor calculations, the refined Nd moments at $B^\pm$ layers and 1.5 K are $2.11(10)\mu_B/\mathrm{Nd}$ ion $(\mathbf{m}[\mathrm{Nd}_1] = (2.05,0,-0.48))$. The refinements (see Fig. 9 and Table II) confirm the direction of these moments nearly parallel to x.

In Fig. 10 we have represented the thermal evolution of the ordered moments in NdNiO_3. At 1.5 K $m(\mathrm{Nd})$ is still not saturated. It is possible to estimate the exchange field seen by Nd^{3+} ions located in $B^\pm$-type magnetic layers in order to determine the antiferromagnetic exchange coupling $J_{\mathrm{Nd-Ni}}$. Without taking into account the crystal-field structure, the simplest way is to consider an exchange magnetic field H_{exc} applied to a temperature-independent moment of saturated value $m_0(\mathrm{Nd})$. In the scope of the mean-field approximation, the exchange magnetic field created by the ordered Ni moments at the site of a Nd atom in a $B^\pm$ layer is given by

$$H_{\mathrm{exc}} = 2zJ_{\mathrm{Nd-Ni}}\langle S_{\mathrm{Ni}}\rangle . \tag{1}$$

Before saturation, the thermal averaged magnetic moment of the Nd atoms is given by

$$\langle m_{\mathrm{Nd}}[T]\rangle = Nm_0(\mathrm{Nd})L(x) ,$$

TABLE II. Experimental and calculated integrated magnetic intensities of PrNiO_3 and NdNiO_3 at 1.5 K. The intensities $I = \sum jL|F_\perp|^2$ are given in barns/unit cell. The calculated intensities for the independent clusters correspond to the magnetic structures model 1 (Ni^{3+} LS equal Ni moments) and model 2 (Ni^{2+} nonequal Ni moments) as detailed in the Appendix.

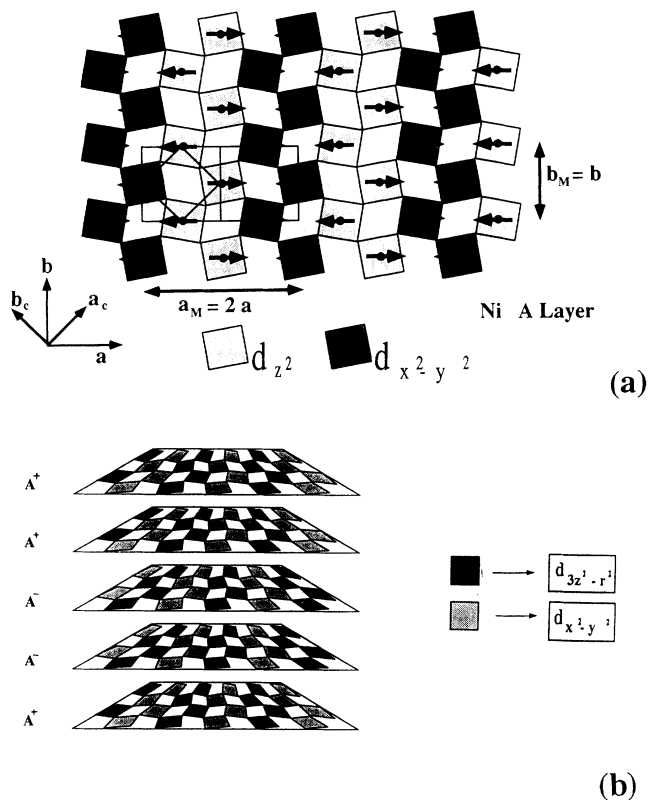| | | | | NdNiO₃ | | PrNiO₃ | |
| | | | | Model 1 | Model 2 | | |
h	k	l	$I_{\mathrm{obs}}(\sigma)$	I_{calc}	I_{calc}	$I_{\mathrm{obs}}(\sigma)$	I_{calc}
1/2	0	1/2	2.9(1.1)	3.4	3.4	7.9(0.4)	8.7
1/2	0	3/2					
1/2	1	1/2	88.6(1.9)	93.9	89.0	12.9(0.4)	13.3
1/2	1	3/2					
3/2	0	1/2	3.3(0.9)	3.7	7.9	5.5(0.5)	5.6
1/2	0	5/2					
3/2	0	3/2					
3/2	1	1/2	25.5(1.7)	26.5	20.1	4.8(0.6)	4.0
1/2	1	5/2					
3/2	1	3/2					
1/2	2	1/2	3.9(0.8)	4.4	8.4	6.1(0.5)	6.5
3/2	0	5/2					
1/2	2	3/2	20.0(1.4)	16.2	15.4	2.3(0.4)	2.6
1/2	1	7/2					
5/2	0	3/2					
1/2	2	5/2					
5/2	1	1/2					
3/2	2	3/2	22.5(2.2)	24.9	22.5	5.0(0.7)	3.9
3/2	0	7/2					
5/2	1	3/2	2.7(1.3)	0.4	0.7		
			$R_{\mathrm{Mag}}(\%)$:	9.6	24.3		8.5

(a)

(b)

FIG. 6. (a) Magnetic arrangement of Ni moments in one of the nickel xy A layers. The different shading of the octahedra would correspond to the occupation of either $d_{3z^2-r^2}$ or $d_{x^2-y^2}$-type orbitals. The crystallographic and magnetic unit cell, as well as the pseudocubic subcell in the (001) plane are displayed. (b) The three-dimensional magnetic ordering consists on the alternance of inverted layers: $A^+ A^+ A^- A^- A^+ A^+ A^- A^- A^+ A^+ \cdots$ along [001].
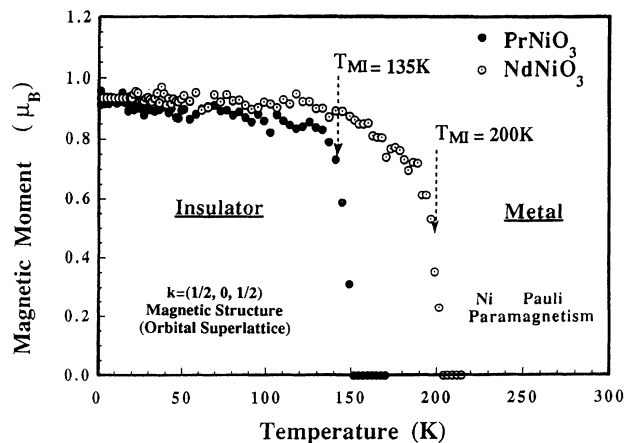

FIG. 7. Temperature dependence of the ordered nickel magnetic moments in PrNiO_3 and NdNiO_3 from the full refinement of the whole diffraction patterns. The first-order-like disappearance of ordered moments of the M-I transition (indicated by arrows) is shown; note the nonsaturated Ni moments in NdNiO_3 above $T \sim 150$ K.
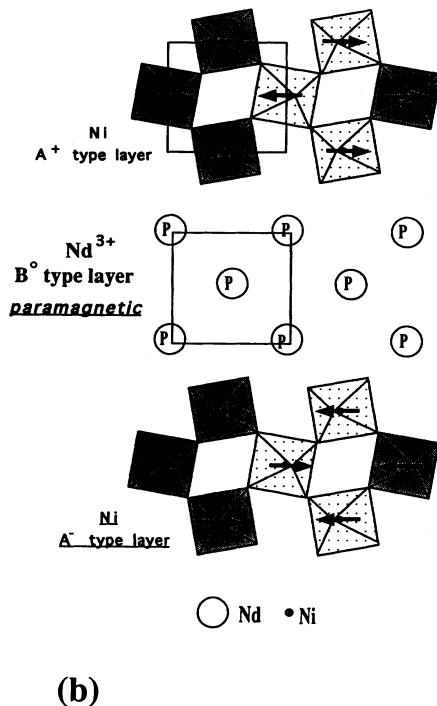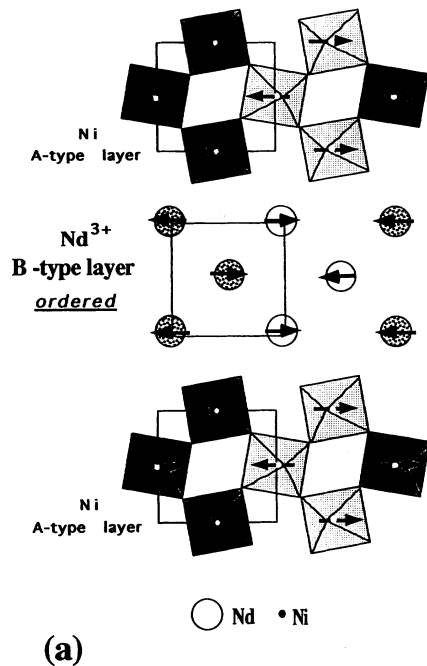
(a)

(b)

FIG. 8. Magnetic ordering of Nd^{3+} ions at low temperatures. Even if Nd only occupies one crystallographic position in the *Pbnm* symmetry, the figure shows the two magnetically different Nd layers resulting from the exchange field created by the nickel magnetic structure: (a) $B^{\pm}$ layers$\rightarrow Nd^{3+}$ moments in between $A^{\pm} - A^{\pm}$ nickel layers are polarized at low temperature. (b) B° layers$\rightarrow Nd^{3+}$ moments in between $A^{\pm} - A^{\mp}$ nickel layers remain paramagnetic. The different shading of the octahedra corresponds to the proposed occupation of either $d_{3z^2-r^2}$ or $d_{x^2-y^2}$-type orbitals.

$L(x)$ being the Langevin function and

$$x = \frac{m_0(Nd)H_{exc}}{k_B T} .$$

Fitting the thermal evolution of the ordered moment $\langle m_{Nd}[t] \rangle$ (Fig. 10) to the above equation, we obtain the value $J_{Nd-Ni} = -0.04(1)$ meV (the minus sign comes from the magnetic structure), and hence $H_{exc} = 2.5(2)$ T, with $m_0(Nd) = 2.7(3)\mu_B$. This antiferromagnetic exchange integral is lower than that between Nd and Ni ions as determined in Nd_2NiO_4 [$J_{Nd-Ni} = -0.6(2)$ meV, Ref. 15], where the polarization effects on the rare earth are already visible below 70–80 K.

Contrary to the behavior of the Kramers Nd^{3+} ion, the neutron-diffraction patterns of $PrNiO_3$ do not show changes associated with the polarization of Pr^{3+} moments at low temperature. This fact is consistent with a singlet ground state of Pr^{3+}. The absence of ordered moments at Pr sites at low temperature, then, is in agreement with the Van Vleck behavior found below ≈ 25 K from susceptibility measurements.[16]

VI. INTERPRETATION OF THE MAGNETIC STRUCTURE: ORBITAL SUPERLATTICE

Before analyzing the relevance of the magnetic structure, we would like to emphasize the implications of our results on the electronic state of the TM ion. One conclusion drawn from photoemission and x-ray absorption spectroscopies on Li-doped NiO and $La_{2-x}Sr_xNiO_4$ ($0 \le x \le 1.15$) (Ref. 10) is that compensating holes have more O $2p$ character than Ni $3d$. In the literature, several spin and charge states for TM bonded to O ions have been proposed, and there is no general agreement about the trivalent state for nickel in systems such as $LiNiO_2$, $NaNiO_2$, $AgNiO_2$, or $LaNiO_3$.[8,9]

From the present neutron-diffraction experiments important conclusions arise, namely the saturated magnetic moment at the Ni site is very close to $1\mu_B$ for both Pr and Nd, compounds and there is no significant magnetic moment at the oxygen sites. This, together with the careful examination of the crystal structure,[1] the magnetic behavior of rare earth, and the analysis of the x-ray absorption experiments,[6] allows us to draw a simple and coherent picture to describe the starting point for the electronic ground state in the insulating regime of $R\,NiO_3$ (R =Pr,Nd). At low temperature the Ni ions behave as ionic low spin Ni^{III} ($S = \frac{1}{2}$). This picture is equivalent to saying that a strong effective crystal field (covalency) overcomes the Hund rule, and the electronic structure of the Ni ions is given, in first approximation, as $\Psi_a = |d^7\rangle = |t_{2g}^6 e_g^1\rangle$. The true ground state should be described by $\Psi_G = \alpha|d^7\rangle + \beta|d^8L\rangle + \gamma|d^9L^2\rangle$ which, neglecting γ, gives a magnetic moment greater than $1\mu_B$ at the Ni site if the zero-point spin reduction of antiferromagnets is neglected. The opposite effect of covalence and spin reduction gives an observed magnetic moment which apparently corresponds to a pure Ni^{III} ($S = \frac{1}{2}$) ionic state. For the following qualitative discussion we adopt the ionic limit $t_{2g}^6 e_g^1$ of E_g symmetry and compati-
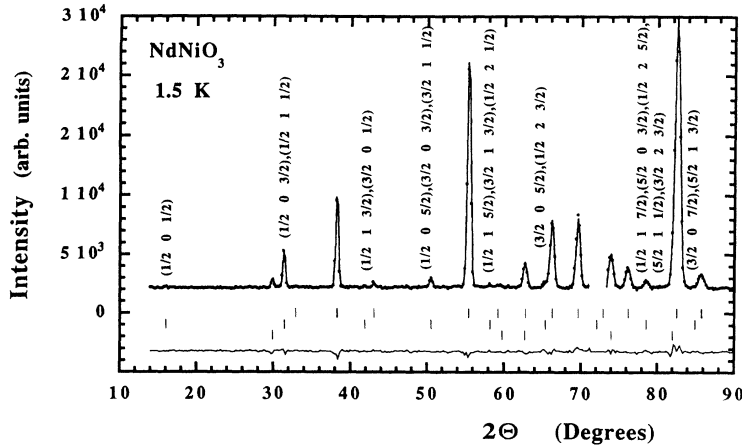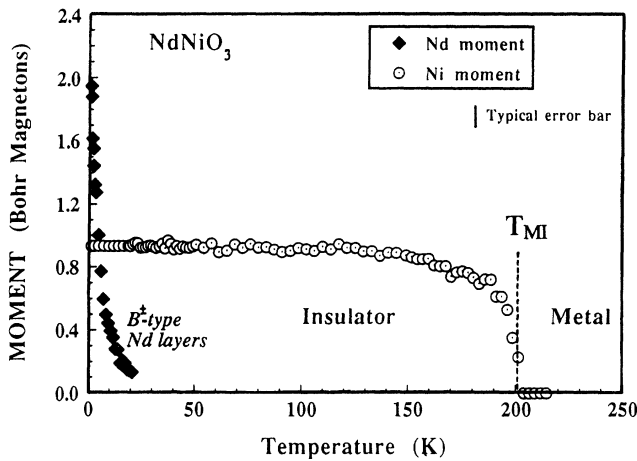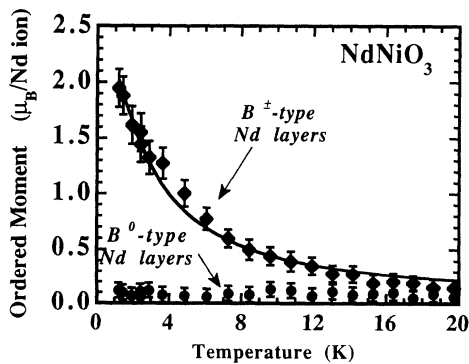
FIG. 9. Details of the refined nuclear and magnetic diffraction patterns of $NdNiO_3$ at 1.5 K by including the Nd and Ni magnetic ordering described in the text.

(a)



(b)

FIG. 10. (a) Temperature dependence of Ni and Nd ordered magnetic moments in $NdNiO_3$ from the refinements. (b) Different thermal evolution of neodymium moments, showing the polarization of Nd^{3+} ions at $B^{\pm}$-type layers, whereas those at B° layers remain paramagnetic (see explanation in the text). The full line corresponds to the mean-field calculations as described in the text.

ble with Jahn-Teller effect.

We want to stress the relevance of the magnetic structure being very different from the expected antiferromagnetically coupled $S = \frac{1}{2}$ Ni^{III} ($t_{2g}^{6}e_{g}^{1}$) spins as proposed by Demazeau et al.[11] for $YNiO_3$ and $LuNiO_3$. To our knowledge, the $\mathbf{k} = (\frac{1}{2}, 0, \frac{1}{2})$ spin arrangement is unique in transition-metal oxides with perovskite structure. As shown in Fig. 6, this wave vector determines a period in the structure which is four times the Ni-Ni distance, and implies the quadrupling of the three cell axes relative to the pseudocubic subcell.

We have to keep in mind that the magnetic structure corresponding to the propagation vector $(\frac{1}{2}, 0, \frac{1}{2})$ cannot be stabilized for nearest-neighbor (NN) exchange integrals of the same sign and absolute values greater than for any other neighbors, which is usually the case for the 180° TM-O-TM exchange topology in perovskite oxides (see, for instance, Ref. 17). Therefore, the only way to stabilize a $(\frac{1}{2}, 0, \frac{1}{2})$ magnetic structure is to accept that NN interactions have different signs as reflected by the magnetic structure: we have as many ferromagnetic couplings (F) between nearest Ni^{III} neighbors as antiferromagnetic (AF) ones (see Fig. 6). And this is in contradiction with a uniform distribution of the single e_g electron. Each Ni is coupled ferromagnetically to three nearest neighbors and antiferromagnetically to the remaining three through the oxygens at the vertices of the octahedra; this is symmetrically achieved, in such a way that F and AF Ni-O-Ni couplings form pairs related by the inversion center at the Ni site in the space group $Pbnm$. *The crystallographic inversion center at the Ni site disappears in the magnetic structure.* The magnetic couplings to a given Ni atom, hereafter labeled $\underline{Ni}$, are identical along the three pseudocubic perovskite axes. For any bonding direction ([1,1,0], [1,−1,0], and [0,0,1]) they are always of the form

$$Ni \ — \ O \ — \ \underline{Ni} \ — \ O \ — \ Ni \ .$$
$$\uparrow \ \cdots F \cdots \ \uparrow \ \cdots AF \cdots \ \downarrow$$
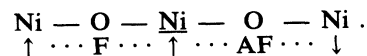
By regarding the electronic configuration of Ni^{III}, with

only one electron in the e_g-type orbitals, we believe that the appearance of such $\mathbf{k}=(\frac{1}{2},0,\frac{1}{2})$ magnetic structure results from the set up of an orbital superlattice. Whereas the t_{2g} orbitals are expected to be fully occupied, the $d_{3z^2-r^2}$ and $d_{x^2-y^2}$ orbitals (forming subbands by hybridization with the O $2p$ orbitals) are probably nondegenerate due to the orthorhombic distortion; but the difference in energy between them may be very small (as suggested by the nearly perfect NiO_6 octahedra[1]), perhaps not very different from the intraatomic ferromagnetic exchange (Hund rule). Considering the weakly interacting Ni atoms in the insulating state (each with one e_g electron apiece) the competition between intraatomic exchange correlations (trying to align neighboring e_g electrons parallel and occupying different orbitals) and the energy gain by the electrons occupying the lower orbital can lead to a ground state in which the lattice breaks up into two sublattices, each with predominantly one of the $d_{3z^2-r^2}$ or $d_{x^2-y^2}$ orbitals half occupied.[18] Thus, from the Goodenough-Kanamori rules, NN Ni atoms with the electron at the same orbital will be AF coupled and those with a different orbital occupancy will prefer to align their $S=\frac{1}{2}$ spins parallel. The different shading of the octahedra in Figs. 6 and 8 corresponds to the proposed different orbital occupation. Cyrot and Lyon-Caen[18] investigated the effects of the orbital degeneracy and intraatomic Coulomb-exchange interactions in narrow band solids by using a doubly degenerate Hubbard model and one electron per atom in a square lattice. They found a ground state consisting of an orbital superlattice (AF orbital ordering).

We call to mind that the high-resolution neutron measurements do not reveal any change in the crystallographic symmetry of the orthorhombic structure (Ref. 1). As there is no significant deformation of the lattice with respect to the metallic phase, we believe that the proposed orbital superlattice may have a different origin from that of $LaMnO_3$ due to the cooperative Jahn-Teller effect.[7] The idea of the pure intra-atomic exchange as responsible for the orbital superlattice, proposed by Cyrot and Lyon-Caen in their simplified model may explain the behavior of $PrNiO_3$ and $NdNiO_3$ below T_{MI}. The concomitant striction-driven distortion of the nuclear structure, if existent, is too small to be observed with our experimental technique.

VII. PHASE DIAGRAM

Finally, let us make some comments on the relationship between the magnetic structure and the metal-insulator transition. Figure 11 displays the phase diagram as a function of the tolerance factor $[t=(d_{R-O})/\sqrt{2}(d_{Ni-O})]$ reported by Torrance et al.,[7] that was completed simply by introducing the unusual magnetic structure below the "metal-magnetic-insulator" boundary. A natural doubt concerns the nature of the still unknown AF ordering in the compounds with $R=$Sm, Eu, Y, and Lu. The nature and sign of the exchange interactions are associated with the orbital ordering, the stability of which seems to be disrupted by the

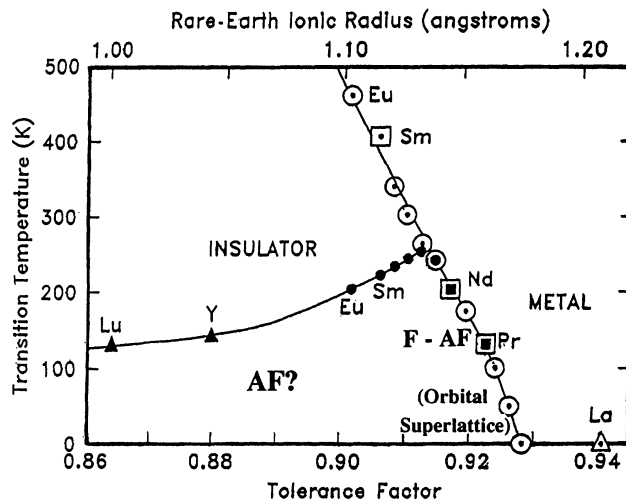FIG. 11. Phase diagram of $R NiO_3$ compounds including the magnetically ordered, metallic and insulator regimes as a function of the tolerance factor $t[t=(d_{R-O})/\sqrt{2}(d_{Ni-O})]$ (modified from Ref. 7). The symmetrical coexistence of F and AF couplings of Ni moments below the "metal-magnetic-insulator" boundary suggest the presence of an orbital superlattice. The nature of the AF ordering in the more distorted compounds ($R=$Sm, Eu, Y, and Lu) is still unknown.

closing of the gap in the compounds with a metal-magnetic-insulator boundary as $PrNiO_3$ and $NdNiO_3$. Then, the formation of the same magnetic structure in the more distorted compounds ($R=$Sm→Lu), for which there is a clear separation between T_N and T_{MI}, is uncertain. Two distinct scenarios can be imagined: (i) The magnetic order is not directly related to the metal-magnetic insulator boundary but to the presence of only one e_g electron. In such a case, the $\mathbf{k}=(\frac{1}{2},0,\frac{1}{2})$ magnetic arrangement should exist as well with $R=$Sm→Lu below T_N. We would expect the special orbital distribution to exist in the insulating but magnetically disordered regime in the more distorted compounds as well. (ii) The usual G-type AF spin configuration $[\mathbf{k}=(0,0,0)]$ occurs with $R=$Sm→Lu due to a uniform ground state and a simple Ni-O-Ni AF coupling. The magnetically ordered region in Fig. 11 would then be split in two subdomains with different antiferromagnetic structures. In such a case the metallic state in $PrNiO_3$ and $NdNiO_3$ compounds should play an important role in the stabilization of the present magnetic structure. The physics of the problem may be, then, related to a spin-density-wave-like behavior.

VIII. SUMMARY AND CONCLUSIONS

Neutron-diffraction experiments and polarization analysis techniques have revealed a sudden formation of localized magnetic moment at Ni sites and ordering in $RNiO_3$ (R:Pr and Nd) across the first-order metal-insulator transition ($\mu_{Ni}\approx0.9\mu_B$; low spin $Ni^{III}t_{2g}^6 e_g^1$ state). A magnetic structure with a wave vector $\mathbf{k}=(\frac{1}{2},0,\frac{1}{2})$ has been discovered in a perovskite oxide.

The propagation vector found implies the quadrupling of the pseudocubic perovskite subcell (with lattice parameters corresponding to one Ni-Ni distance) along the three axes. In $PrNiO_3$ and $NdNiO_3$ this magnetic superstructure necessarily implies the disappearance of the inversion center at Ni site in the $Pbnm$ space group, and is in contradiction with a uniform distribution of the single e_g electron. The observed symmetrical coexistence of ferro and antiferromagnetic couplings suggests the existence of an orbital superlattice which may result from the breakdown of the degeneracy of the e_g^1 state due to electronic correlation. These conclusions are also corroborated by the magnetic behavior of Nd ions. Further experimental work is required to investigate the possible extensions of some of these conclusions to the more distorted $R\,NiO_3$ compounds.

ACKNOWLEDGMENTS

APPENDIX: DESCRIPTION OF POSSIBLE MAGNETIC STRUCTURES BASED ON GROUP THEORY

The possible magnetic structures have been studied by using group theory. The method, developed by Bertaut[19] and extended by many others (see for instance Ref. 20), consists of looking for the irreducible representations

(irep) of the wave-vector group and their basis functions that describe the possible magnetic structures. For each combination of basis functions, one has to systematically check the agreement between the observed and calculated diffraction patterns.

The wave vector $\mathbf{k}=(\frac{1}{2},0,\frac{1}{2})$ is referred to the conventional crystallographic reciprocal basis and corresponds to the point T of the Brillouin zone.[21] The wave-vector group coincides with the whole space group because $\mathbf{k}$ is invariant under all the point-group symmetry operations: $G_{\mathbf{k}}=Pbnm$. The ireps of a nonsymmorphic space group, as $Pbnm$, when the wave vector belongs to the surface of the Brillouin zone, are not easy to obtain. The representations can be found by different methods: one can consult the tables given by Bradley and Cracknell[21] or those by Kovalev[22] or use the program KAREP,[23] for instance, or deduce the representations by hand. All of these methods give the same result (or equivalent, by a similarity transformation). We shall follow Ref. 19, where an explicit method is given for finding all the representations of $G_{\mathbf{k}}=Pbnm$, $\mathbf{k}$ being an invariant point at the surface of the Brillouin zone. All the relevant information concerning the explicit form of the ireps of $Pbnm$ for $\mathbf{k}=(\frac{1}{2},0,\frac{1}{2})$ is summarized in Table III.

In Table IV we give the basis functions of the two ireps for the special positions occupied by the Ni atoms and the rare earth, obtained by applying standard projection operators formulas. Three sets of basis functions (corresponding to the three directions x,y,z) are generated, because the magnetic reducible representation[19,20] contains three times each irep. Two notations are used, the numeric form corresponds to the "atomic vector components" of the basis functions as defined by Yzyumov

TABLE III. Representations of the space group $G_{\mathbf{k}=(1/2,0,1/2)}=Pbnm$ obtained with the method of Ref. 19. The explicit form of the $Pbnm$ symmetry operators is given in a notation based in Hermann-Mauguin symobls (IT), as well as in Bradley and Cracknell (BC) and Kovalev's (K) notations (only rotational part is given).

Coset representatives, relationships with the generators, $\{2_{1x},2_{1y},\bar{1}\}$ (GR), and equivalent positions (EP) of $G=Pbnm$.

K	IT	BC	GR	EP
h_1	1	$\{1\|000\}$	1	(x,y,z)
h_2	2_{1x}	$\{C_x\|\frac{1}{2}\frac{1}{2}0\}$	2_{1x}	$(\frac{1}{2}+x,\frac{1}{2}-y,-z)$
h_3	2_{1y}	$\{C_y\|\frac{1}{2}\frac{1}{2}\frac{1}{2}\}$	2_{1y}	$(\frac{1}{2}-x,\frac{1}{2}+y,\frac{1}{2}-z)$
h_4	2_{1z}	$\{C_z\|10-\frac{1}{2}\}$	$2_{1x}\cdot2_{1y}$	$(1-x,-y,-\frac{1}{2}+z)$
h_{25}	$\bar{1}$	$\{\bar{1}\|000\}$	$(\bar{1})$	$(-x,-y,-z)$
h_{26}	b	$\{\sigma_x\|\frac{1}{2}\frac{1}{2}0\}$	$2_{1x}\cdot(\bar{1})$	$(\frac{1}{2}-x,\frac{1}{2}+y,z)$
h_{27}	n	$\{\sigma_y\|\frac{1}{2}\frac{1}{2}\frac{1}{2}\}$	$2_{1y}\cdot(\bar{1})$	$(\frac{1}{2}+x,\frac{1}{2}-y,\frac{1}{2}+z)$
h_{28}	m	$\{\sigma_z\|10-\frac{1}{2}\}$	$2_{1x}\cdot2_{1y}\cdot(\bar{1})$	$(1+x,y,-\frac{1}{2}-z)$

Representations can be written in terms of the following two-dimensional matrices:

$$I=\begin{bmatrix}1 & 0\\0 & 1\end{bmatrix}, \qquad A_1=\begin{bmatrix}0 & 1\\\bar{1} & 0\end{bmatrix}, \qquad A_2=\begin{bmatrix}0 & 1\\1 & 0\end{bmatrix}, \qquad A_3=\begin{bmatrix}1 & 0\\0 & \bar{1}\end{bmatrix}.$$

Matrices of the two irreducible representations (T_1,T_2):

	1	2_{1x}	2_{1y}	2_{1z}	$\bar{1}$	b	n	m
T_1	I	A_1	$-I$	$-A_1$	A_2	A_3	$-A_2$	$-A_3$
T_2	I	A_1	I	A_1	A_2	A_3	A_2	A_3

and co-workers,[20] and the symbolic one (F, G, A, C) corresponds to the linear combinations of magnetic moments attached to each sublattice of a Wyckoff site, as used by Bertaut.[19]

The possible magnetic structures can be represented by linear combinations of atomic vector components of the basis functions given in Table IV. Combination of basis functions of the two representations should also be considered, as the magnetic ordering appears in a first-order phase transition. For a particular, Wyckoff site, with several sublattices, the component $\alpha\,(=x,y,z)$ of the magnetic moment at the sublattice "i" within the reference cell is given by

$$m_{i\alpha}(0)=\sum_{\nu\lambda\alpha}M^{\nu}_{\lambda\alpha}\Psi^{\nu}_{\lambda\alpha}(i)\,,\qquad\text{(A1)}$$

where the indices $\nu\,(=1,2)$ and $\lambda\,(=1,2)$ label the ireps and the different partners (equal to the dimension of the irep). The magnetic moments in the unit cell with origin in the lattice point $\mathbf{R}$ are related to those within the unit cell at the origin by

$$\mathbf{m}_i(\mathbf{R})=\mathbf{m}_i(0)\exp\{2\pi\mathbf{k}\cdot\mathbf{R}\}\,.\qquad\text{(A2)}$$

The mixing coefficients $M^{\nu}_{\lambda\alpha}$ have to be determined from the experiment and determine the magnitude and direction of the magnetic moments. It is clear that two-dimensional ireps allow linear combination of basis functions that can lead to magnetic structures with nonequal magnetic moments.[20] If different partners are mixed, within the same or different ireps of the basis functions given in Table IV, with equal coefficients non-equal-

TABLE IV. Basis functions.

Basis functions for Ni site Ni$_1$($\tfrac{1}{2}$,0,0), Ni$_2$($\tfrac{1}{2}$,0,$\tfrac{1}{2}$), Ni$_3$(0,$\tfrac{1}{2}$,$\tfrac{1}{2}$), and Ni$_4$(0,$\tfrac{1}{2}$,0).

		Ni$_1$	Ni$_2$	Ni$_3$	Ni$_4$	
T_1	$\Psi_1^{T_1}$	(100)	(100)	(100)	(100)	
		(010)	(010)	(0$\bar{1}$0)	(0$\bar{1}$0)	(F_x,C_y,G_z)
		(001)	(00$\bar{1}$)	(001)	(00$\bar{1}$)	
	$\Psi_2^{T_1}$	(100)	($\bar{1}$00)	(100)	($\bar{1}$00)	
		(010)	(0$\bar{1}$0)	(0$\bar{1}$0)	(010)	(G_x,A_y,F_z)
		(001)	(001)	(001)	(001)	
T_2	$\Psi_1^{T_2}$	(100)	($\bar{1}$00)	($\bar{1}$00)	(100)	
		(010)	(0$\bar{1}$0)	(010)	(0$\bar{1}$0)	(A_x,G_y,C_z)
		(001)	(001)	(00$\bar{1}$)	(00$\bar{1}$)	
	$\Psi_2^{T_2}$	(100)	(100)	($\bar{1}$00)	($\bar{1}$00)	
		(010)	(010)	(010)	(010)	(C_x,F_y,A_z)
		(001)	(00$\bar{1}$)	(00$\bar{1}$)	(001)	

where $\mathbf{F}=\mathbf{m}_1+\mathbf{m}_2+\mathbf{m}_3+\mathbf{m}_4$, $\mathbf{G}=\mathbf{m}_1-\mathbf{m}_2+\mathbf{m}_3-\mathbf{m}_4$, $\mathbf{C}=\mathbf{m}_1+\mathbf{m}_2-\mathbf{m}_3-\mathbf{m}_4$, $\mathbf{A}=\mathbf{m}_1-\mathbf{m}_2-\mathbf{m}_3+\mathbf{m}_4$.

Basis functions for the rare-earth site (real representation)
$R_1(x,y,\tfrac{1}{4})$, $R_2(1-x,1-y,\tfrac{3}{4})$, $R_3(x-\tfrac{1}{2},\tfrac{3}{2}-y,\tfrac{3}{4})$, and $R_4(\tfrac{3}{2}-x,y-\tfrac{1}{2},\tfrac{1}{4})$.
$\mathbf{V}^{\pm}=S_1\pm S_4$ $\mathbf{W}^{\pm}=S_2\pm S_3$

		R_1	R_2	R_3	R_4	
T_1	$\Psi_1^{T_1}$	(100)	0	0	($\bar{1}$00)	
		(010)	0	0	(010)	(V_x^-,V_y^+,V_z^-)
		(001)	0	0	(00$\bar{1}$)	
	$\Psi_2^{T_1}$	0	(100)	($\bar{1}$00)	0	
		0	(010)	(010)	0	(W_x^-,W_y^+,W_z^-)
		0	(001)	(00$\bar{1}$)	0	
T_2	$\Psi_1^{T_2}$	(100)	0	0	(100)	
		(010)	0	0	(0$\bar{1}$0)	(V_x^+,V_y^-,V_z^+)
		(001)	0	0	(001)	
	$\Psi_2^{T_2}$	0	(100)	(100)	0	
		0	(010)	(0$\bar{1}$0)	0	(W_x^+,W_y^-,W_z^+)
		0	(001)	(001)	0	

with $\mathbf{V}^{\pm}=\mathbf{m}_1\pm\mathbf{m}_4$ $\mathbf{W}^{\pm}=\mathbf{m}_2\pm\mathbf{m}_3$.

moment magnetic structures can be obtained for the case of the Ni site. For instance, $M^{\gamma}_{1\alpha}=M^{\gamma}_{2\alpha}(\forall\nu,\alpha)$ implies that only two of the four Ni ions have an ordered magnetic moment. The same condition applied to Nd site gives an equal-moment magnetic structure for Nd sublattices.

There are no general extinction rules for the propagation vector $\mathbf{k}=(\frac{1}{2},0,\frac{1}{2})$ in the case of ordering of both sites R and Ni. The magnetic structure factor (for the Ni sublattices) for a reflection $\mathbf{Q}/2\pi=\mathbf{H}+\mathbf{k}=(h+\frac{1}{2},k,l+\frac{1}{2})$ is given by

$$\mathbf{F}(\mathbf{H}+\mathbf{k})=\mathbf{F}(h+\tfrac{1}{2},k,l+\tfrac{1}{2})$$
$$=f(\mathbf{H}+\mathbf{k})\{\mathbf{m}_4(-1)^k-\mathbf{m}_2(-1)^{h+l}$$
$$+i[\mathbf{m}_1(-1)^n+\mathbf{m}_3(-1)^{k+l}]\}\ .$$
$$\text{(A3)}$$

The intensity is proportional to the square of the perpendicular component of $\mathbf{F}$ to the scattering vector $\mathbf{Q}$, $I\approx|\mathbf{F}_{\perp}|^2$. Calling $\mathbf{q}_i=\mathbf{e}\times\mathbf{m}_i\times\mathbf{e}$, where $\mathbf{e}=\mathbf{Q}/Q$, the intensity is given by,

$$I\approx f^2(\mathbf{H}+\mathbf{k})\left\{\sum q_i^2+2(-1)^{h+k+l}[\mathbf{q}_1\mathbf{q}_3-\mathbf{q}_2\mathbf{q}_4]\right\}\ ,\quad\text{(A4)}$$

which could be zero only for special values and orientations of $\mathbf{q}_i$. For collinear structures, $q_i=\pm q=\pm m\sin\alpha$ (α is the angle between the easy axis and $\mathbf{Q}$), one has

$$I\approx 2f^2(\mathbf{H}+\mathbf{k})q^2\{2+(-1)^{h+k+l}[\eta_{13}-\eta_{24}]\}\ ,\quad\text{(A5)}$$

where $\eta_{ij}=1$ if the atoms i and j have parallel moments and $\eta_{ij}=-1$ if the atoms i and j have antiparallel moments. It can be seen right away that the intensity of collinear F, G, A, and C modes ($\eta_{13}=\eta_{24}$) are identical $I_{\text{FGAC}}\approx 4f^2(\mathbf{H}+\mathbf{k})q^2$, because they represent identical magnetic structures for the propagation vector $\mathbf{k}=(\frac{1}{2},0,\frac{1}{2})$. A simple change of the origin renumbers the atoms in such a way as to change the "label" of the magnetic mode.

Expression (A5) can be identically zero for $\eta_{13}=-\eta_{24}=1$ and $h+k+l=2n+1$ (or in the case $\eta_{13}=-\eta_{24}=-1$ and $h+k+l=2n$) that corresponds to three atoms of the chemical unit cell having the same magnetic moment antiparallel to the fourth one. Such configurations are indistinguishable from those of F, G, A, or C modes for powder samples. The reason (for $\eta_{13}=-\eta_{24}=1$) is that reflections $\mathbf{H}+\mathbf{k}$, with $h+k+l=2n$, of intensity $I\approx 2I_{\text{FGAC}}$ appears to overlap with those with null intensities. A configuration of type $(+++-)$ corresponds to a relative shift, $\mathbf{t}=[\frac{1}{2},\frac{1}{2},0]$ of two consecutive A layers (Fig. 6).

The total number of independent magnetic reflections in the accessible half reciprocal sphere (D1B, $\lambda=2.52$ Å, $2\theta_{\max}=85°$) is 64, but due to the weakness of the magnetic reflections and to the powder samples we dispose of a small number of observations: only six (eight) clusters with a single integrated intensity can be used to solve the magnetic structure for $PrNiO_3$ ($NdNiO_3$). Of course, the

refinement of the model with the Rietveld method takes into account all the reflections.

The determination of the magnetic structure was first performed by a trial and error method selecting particular values of the coefficients $M^{\gamma}_{\lambda\alpha}$ in order to reproduce the experimental intensities. Second, a program based in the "simulated annealing" (SA) optimization method[24] was used to study the "degeneracy" of the solutions, that is, the different magnetic orderings compatible with the observed pattern. This program applies the Metropolis algorithm for a search in the configurational space of the orientation and magnitude of the magnetic moments minimizing the R factor. After an exhaustive analysis we realized that several solutions gave nearly the same powder pattern for the case of $PrNiO_3$. Many of them correspond to a change of the origin (as discussed above for collinear structures) or to pseudo "configurational domains" coming from the pseudocubic character of these perovskites: the propagation vector in the corresponding cubic subcell is $(\frac{1}{4},\frac{1}{4},\frac{1}{4})$ which has an eight-armed star. In all cases the y component was nearly zero and the values $M^{\gamma}_{\lambda y}=0$ ($\forall\nu,\lambda$), were assumed for the subsequent analysis. The best equal-moment solution is $(F_x,0,G_z\approx 0)$ that corresponds to the first partner of the irep T_1. However, the second partner $(G_x\approx 0,0,F_z)$ gave very similar results. The saturated magnetic moment at the Ni site for these solutions was $0.90(2)\mu_B$ at 1.5 K.

Another magnetic ordering compatible with the observed diffraction pattern is that corresponding to non-equal-moment magnetic structures.[25] Only two of the four Ni atoms in a primitive cell have a moment $\mu_{\text{Ni}}\approx 1.8\mu_B$. The appealing feature of this alternative view is that the Ni ions can be considered as split into two kinds of nonequivalent Ni^{2+} species: Ni^{2+}-$HS(t^6_{2g}d^1_{z^2}d^1_{x^2-y^2})$ and diamagnetic Ni^{2+}-$LS(t^6_{2g}d^2_{z^2}d^0_{x^2-y^2})$. The drawback is that no evidence of the coexistence of these two states has been found in the analysis of the crystal structure.[1]

The combined ordering of Nd and Ni moments below 20 K in $NdNiO_3$ clearly breaks the degeneracy of the solutions for the Ni ordering found in $PrNiO_3$ (and in $NdNiO_3$ at higher temperatures). A careful analysis, using the SA technique,[24] was performed in order to determine whether the observed magnetic intensities of $NdNiO_3$ at 1.5 K were compatible with the non-equal-moment structure for Ni, i.e., two kinds of electronic configurations (HS and diamagnetic LS) for eventual Ni^{2+} ions. We have explored many configurations constraining only the value of the Ni moments and the results can be reduced basically to the two following models.

Model 1 (Low-spin Ni^{3+}): Ni sublattices coupled according to the basis functions $(F_x,0,G_z)$ and moments fixed. All $M^{\gamma}_{\lambda\alpha}=0$, except M^1_{1x} and M^1_{1z}, which were constrained to give $m(\text{Ni})=0.9\mu_B$. The Nd sublattices were divided into two types of sites, one with zero moments $m(\text{Nd}_2)=m(\text{Nd}_3)=0$ and the other with equal moments $m(\text{Nd}_1)=m(\text{Nd}_4)$. Corresponding to the basis function $(V^-_x,0,V^-_z)$, i.e., all $M^{\gamma}_{\lambda\alpha}=0$ except M^1_{1x} and M^1_{1z}.

Model 2 (High-spin Ni^{2+} and low-spin Ni^{2+}): The Ni atoms 2 and 4 were attributed a zero moment: $M^1_{1a} = M^1_{2a}$ and $M^2_{\lambda a} = 0$, with the value $m(Ni_1) = m(Ni_3) = 1.8\mu_B$. The four Nd sublattices were constrained to have the same magnetic moment: $M^1_{1a} = M^1_{2a}$ and $M^2_{\lambda a} = 0$, or $M^2_{1a} = M^2_{2a}$ and $M^1_{\lambda a} = 0$.

Model 1 gives the best result and corresponds simply to a magnetic structure where the two types of magnetic sites existing in the compound are coupled within the same irep. The results are summarized in Table I.

The best result obtained with Model 2 corresponds to the following values for the reference atoms:

Ni site: $\Psi^{T1}_1 + \Psi^{T1}_2$

$$= 2(m_{1x} - m_{3x}, m_{1y} + m_{3y}, m_{1z} - m_{3z}),$$

$$m(Ni_1) \approx (0.42, 0, 1.75),$$

Nd site: $\Psi^{T1}_1 + \Psi^{T1}_2 = 2(C_x, F_y, C_z),$

$$m(Nd_1) \approx (0.7, 0, 1.5), \quad m(Nd) \approx 1.7\mu_B$$

The observed and calculated integrated intensities of the best fits for the two models, obtained with the SA pro-

cedure, are shown in Table II.

A more general variant of Model 1 was also explored. The Nd sublattices were divided in two types of sites with two undetermined moments, the coupling between the two Nd atoms within each site was also a variable in the SA procedure: all $M^\gamma_{\lambda a}$ are variable except $M^\gamma_{\lambda y} = 0$ and the constraint giving a common moment for Nd_1 and Nd_4, as well as for Nd_2 and Nd_3. The SA method converged towards Model 1, as presented above: in different runs the magnetic moment for the pairs Nd_2-Nd_3 was found to be negligible within the experimental error.

The above considerations led us to conclude that the magnetic structure in $NdNiO_3$ is that described by equal Ni moments and nonequal Nd moments (Model 1). If we assume a similar Ni-moment orientation in $PrNiO_3$, we can also conclude that the magnetic structure should correspond to the first one, $\approx F_x$ and $m(Ni) = 0.9\mu_B$.

The fine details of the magnetic structure in both compounds could be determined only by using single crystals, which are not available at present, and polarized neutrons. However, the main physical consequence of the magnetic ordering in this system, the orbital superlattice, is largely determined by the propagation vector itself.

*Permanent address: Laboratoire des Fluorures, Université du Maine, Avenue Olivier-Messiaen, 72017 Le Mans Cedex, France.

[1]J. L. García-Muñoz, J. Rodríguez-Carvajal, P. Lacorre, and J. B. Torrance, Phys. Rev. B 46, 4414 (1992).

[2]P. Lacorre, J. B. Torrance, J. Pannetier, A. I. Nazzal, P. W. Wang, T. C. Huang, and R. L. Siemens, J. Solid State Chem. 91, 225 (1991).

[3]H. J. de Boer and E. J. W. Verwey, Proc. Phys. Soc. London Sect. A 49, 59 (1937).

[4]J. Zaanen, G. A. Sawatzky, and J. W. Allen, Phys. Rev. Lett. 55, 418 (1985).

[5]J. B. Torrance, P. Lacorre, C. Ansavaroengchai, and R. M. Metzger, J. Solid State Chem. 90, 168 (1991); Physica C 182, 351 (1991).

[6]M. Medarde, J. L. García-Muñoz, A. Fontaine, J. Rodríguez-Carvajal, M. de Santis, M. Sacchi, G. Rossi, and P. Lacorre, Phys. Rev. B 46, 14 975 (1992).

[7]J. B. Torrance, P. Lacorre, A. I. Nazzal, E. J. Ansaldo, and Ch. Niedermayer, Phys. Rev. B 45, 8209 (1992).

[8]T. Mizokawa, H. Namatame, A. Fujimori, K. Akeyama, H. Kondoh, H. Kuroda, and N. Kosugi, Phys. Rev. Lett. 67, 1638 (1991).

[9]G. Ranga Rao, M. S. Hegde, D. D. Sarma, and C. N. R. Rao, J. Phys. Condens. Matter 1, 2147 (1989).

[10]P. Kuiper, G. Kruizinga, J. Ghijsen, and G. A. Sawatzky, Phys. Rev. Lett. 62, 221 (1989); also P. Kuiper, J.v. Elp, J. G. A. Sawatzky, A. Fujimori, S. Hosoya, and D. M. Leeuw, Phys. Rev. B 44, 4570 (1991).

[11]G. Demazeau, A. Marbeuf, M. Pouchard, and P. Hagenmuller, J. Solid State Chem. 3, 582 (1971).

[12]J. L. García-Muñoz, J. Rodríguez-Carvajal, and P. Lacorre, Europhys. Lett. 20, 241 (1992).

[13]J. Rodríguez, M. Anne, and J. Pannetier (unpublished).

[14]J. Rodríguez-Carvajal, FULLPROF: A Program for Rietveld Refinement and Pattern Matching Analysis, Abstract of the

Satellite Meeting of the XVth Congress of the International Union of Crystallography, Toulouse, France, 1990 (Université Paul Sabatier, Toulouse, 1990), p. 127.

[15]J. Rodríguez-Carvajal, T. Fernández, J. L. Martínez, F. Fernández, and R. Sáez-Puche, Europhys. Lett. 11(3), 261 (1990); See also X. Batlle, X. Obradors, and B. Martínez, Phys. Rev. B 45, 2830 (1992).

[16]J. L. García-Muñoz et al. (unpublished).

[17]J. B. Goodenough and J. M. Longo, in Magnetic and Other Properties in Oxides and Related Compounds, edited by K. H. Hellwege and A. M. Hellwege, Landolt-Börnstein, New Series, Group III, Vol. 4a (Springer-Verlag, Berlin, 1970), Chap. 3.

[18]M. Cyrot and C. Lyon-Caen, J. Phys. (Paris) 36, 253 (1975).

[19]E. F. Bertaut, Magnetism, edited by G. T. Rado and H. Shul (Academic, New York, 1963), Vol. III, Chap. 4, p. 149; See also, Acta Crystallogr. A 24, 217 (1968); J. Phys. (Paris) Colloq. 32, C1-462 (1971); J. Magn. Magn. Mater. 24, 267 (1981).

[20]Y. A. Izyumov and V. E. Naish, J. Magn. Magn. Mater. 12, 239 (1979); Y. A. Izyumov, V. E. Naish, and V. N. Syromiatnikov, ibid. 12, 249 (1979); Y. A. Izyumov, V. E. Naish, and S. B. Petrov, ibid. 13, 267 (1979); 13, 275 (1979); Y. A. Izyumov, ibid. 21, 33 (1980).

[21]C. J. Bradley and A. P. Cracknell, The Mathematical Theory of Symmetry in Solids (Clarendon, Oxford, 1972).

[22]O. V. Kovalev, Irreducible Representations of the Space Groups (Gordon and Breach, New York, 1965).

[23]E. Hovestreydt, M. Aroyo, S. Sattler, and H. Wondratschek, J. Appl. Crystallogr. 25, 544 (1992).

[24]J. Rodríguez-Carvajal, Physica B 192, 55 (1993).

[25]The fact that we can obtain only two Ni/cell with ordered moments and the same R factors as the equal-moment magnetic structure can be easily understood considering the simplified model of a simple Bravais lattice as in the case of the cubic perovskite. For a sinusoidal magnetic structure described by the Fourier component $m_k = A/2 \exp[i\phi]u$, the

magnetic moment in planes perpendicular to the propagation vector $\mathbf{k}=(\frac{1}{4},\frac{1}{4},\frac{1}{4})$, is given by $\mathbf{m}_p = A\cos(2\pi\mathbf{k}\mathbf{R}+\phi)\mathbf{u}$ $= A\cos(p\pi/2+\phi)\mathbf{u}$ with $\mathbf{p}\in Z$. The intensity of a magnetic reflection for the scattering vector $\mathbf{Q}=2\pi(\mathbf{H}+\mathbf{k})$ is proportional to $|\mathbf{F}_{\perp}|^2=|\mathbf{m}_k|^2-|(\mathbf{m}_k\mathbf{Q})\mathbf{Q}/Q^2|^2$ which does not depend on ϕ. For $\phi=0$ the magnetic moments in consecutive planes perpendicular to $\mathbf{k}$ follow the sequence $(+0-0+0-0\cdots)$, where the non-null moments have a magnitude $m_0 = A$. For $\phi=(2n+1)\pi/4$, all the moments have the same magnitude, $m_0 = A/\sqrt{2}$, and the sequence is $(++--++--\cdots)$. Both configurations are indistinguishable by neutron-scattering experiments. If one considers collinear structures, from formula (A5) is easy to see that by putting two atoms with null moments it is always possible to get a solution for $q = m\sin\alpha$.
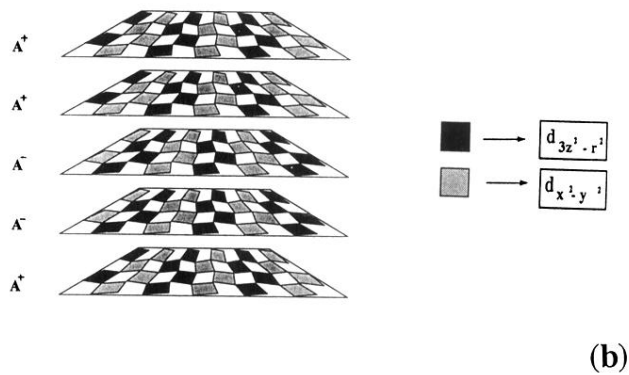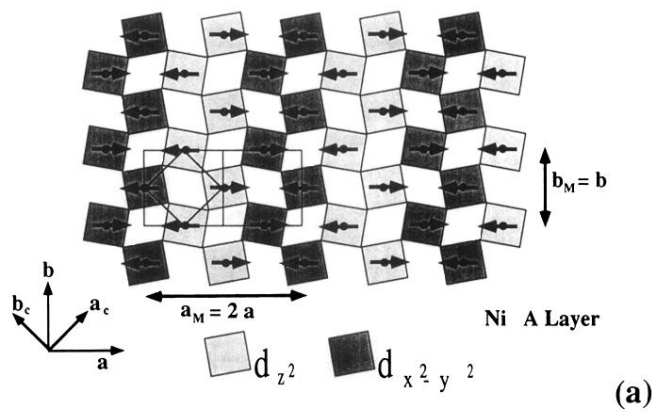
FIG. 6. (a) Magnetic arrangement of Ni moments in one of the nickel xy A layers. The different shading of the octahedra would correspond to the occupation of either $d_{3z^2-r^2}$ or $d_{x^2-y^2}$-type orbitals. The crystallographic and magnetic unit cell, as well as the pseudocubic subcell in the (001) plane are displayed. (b) The three-dimensional magnetic ordering consists on the alternance of inverted layers: $A^+A^+A^-A^-A^+A^+A^-A^-A^+A^+ \cdots$ along [001].
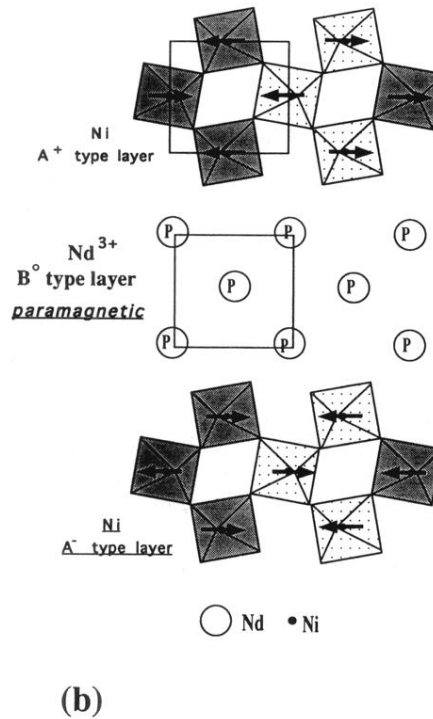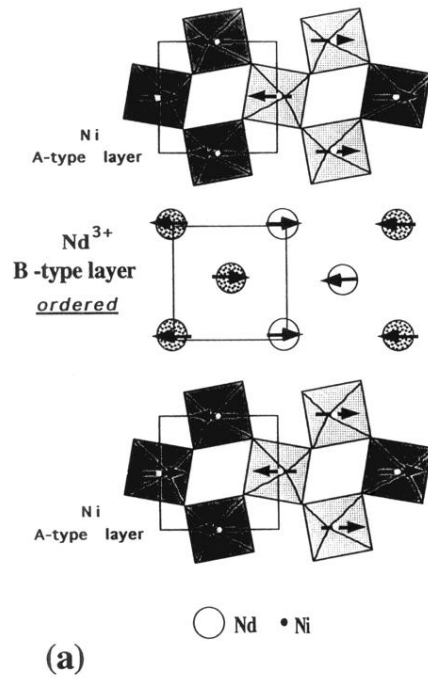
FIG. 8. Magnetic ordering of Nd^{3+} ions at low temperatures. Even if Nd only occupies one crystallographic position in the *Pbnm* symmetry, the figure shows the two magnetically different Nd layers resulting from the exchange field created by the nickel magnetic structure: (a) $B^{\pm}$ layers→Nd^{3+} moments in between $A^{\pm} - A^{\pm}$ nickel layers are polarized at low temperature. (b) B° layers→Nd^{3+} moments in between $A^{\pm} - A^{\mp}$ nickel layers remain paramagnetic. The different shading of the octahedra corresponds to the proposed occupation of either $d_{3z^2-r^2}$ or $d_{x^2-y^2}$-type orbitals.